PROCEEDINGS OF THE ROYAL SOCIETY A

Proc. R. Soc. A (2007) **463**, 1509–1523
doi:10.1098/rspa.2007.1836
Published online 20 March 2007

Modelling real-time dynamic substructuring using partial delay differential equations

By Y. N. Kyrychko[1,*], S. J. Hogan[1], A. Gonzalez-Buelga[2] and D. J. Wagg[2]

[1]*Department of Engineering Mathematics, and* [2]*Department of Mechanical Engineering, University of Bristol, Queen's Building, Bristol BS8 1TR, UK*

Real-time dynamic substructuring is a new component testing method for simulating the dynamics of complex engineering systems. The physical component is tested within a computer-generated 'virtual' environment using real-time control techniques. Delays in communication which occur between the component and the virtual environment can potentially destabilize the simulation. In this paper, the mechanism for this instability is examined using a beam-oscillator system as a case study. We will show how the stability and the amplitude response of the system change with the time delay. Numerical simulations of the reduced system as well as a full-delayed beam equation are performed. A series of experimental tests is carried out on a beam-oscillator system. Comparison of the theoretical, numerical and experimental results is presented and these agree remarkably well.

Keywords: beam-oscillator system; real-time dynamic substructuring; delay equations; hybrid testing

1. Introduction

The main methods of testing the response of the structures under external loads and excitations (e.g. earthquake testing techniques) are shaking tables, pseudo-dynamic testing and real-time dynamic substructuring (Blakeborough *et al.* 2001; Williams & Blakeborough 2001). Every method has its advantages and limitations. In particular, shaking tables are usually expensive to build and operate, and the structures have to be scaled down. This reduces the understanding of the structural response as scaling down the structures leads to a non-commensurate change of material properties of the original system. Pseudo-dynamic testing is not done in real time and this leads to lengthy and costly experiments.

On the other hand, recent advances in analytical and numerical methods have led to further development of real-time dynamic substructuring. The structure to be tested or emulated is first divided into two parts. One part is placed in the laboratory and another one is modelled numerically. The parts are usually connected by electric or hydraulic actuators, which introduce the interface forces between computational and experimental parts. The actuators act as a transfer system and are designed to follow appropriate output displacements calculated by the numerical model (Wallace *et al.* 2005; Kyrychko *et al.* 2006).

* Author for correspondence (y.kyrychko@bristol.ac.uk).

Received 8 August 2006
Accepted 21 February 2007

The main advantage of this technique is that experiments are not very expensive to build, they run in real time, and are repeatable. This technique also allows parametric variation of numerical model parameters and can be applied not only to test the structural response under an earthquake, but also to test parts of machinery, cars, etc. (Williams & Blakeborough 2001). Also in this way, the numerical, analytical and experimental techniques are tied together, and this helps to better understand the behaviour of the model under consideration. Potentially, real-time dynamic substructuring can be performed online in different places, even in different countries.

The main challenge is to ensure that the substructured system behaves in the same way as the emulated system. The transfer systems typically introduce a time lag or delay into the system, and this effect must be accounted for while performing a real-time dynamic substructuring experiment. Recently, it was suggested that the way to analytically model a dynamic substructuring experiment is to use delay differential equations (DDEs; see, for instance, Wallace *et al.* 2005; Kyrychko *et al.* 2006). Thus, the system is modelled more realistically, and therefore should lead to more reliable results. Unfortunately, time delay can lead to a complete destabilization of the system but artificial variation of the delay time may help one to change from an unstable to a stable regime. Owing to the infinite dimensionality of the DDEs, inclusion of time delays into the equation of motion makes analysis more difficult and challenging. The theory of the equations with time-delays is an active topic of research and some recent developments can be found in, for example, Hu & Wang (2002), Adimy *et al.* (2006) and Laurent *et al.* (2006).

In this paper, we introduce a system which consists of a clamped-free cantilever beam, with a mass-spring-damper (MSD) attached to the free end of the beam. There are many applications of such system, including vibrations of elastic arms and their suppression, robotics, vibrations of vehicle on a compressed rail, etc. An analytical and experimental investigation of beams carrying elastically mounted masses was performed by Ercoli & Laura (1987). Rossi *et al.* (1993) have found the exact solution of the free vibrations of Timoshenko beams carrying elastically mounted masses. Gürgöze has derived the frequency equation for the cantilever beam with attached tip mass and a spring mass (Gürgöze 1996) and studied the sensitivity of the eigenvalues of a viscously damped cantilever beam carrying a tip mass (Gürgöze 1998). The question of controlling hybrid experiments in which only some of the state variables are accessible for measurements, has been investigated by Sieber & Krauskopf (in press). Our stability findings will provide a background for implementing this control technique in a real experiment.

We propose to implement real-time dynamic substructuring in this system by modelling a MSD connected via a transfer system to the beam placed in the laboratory, with the force being generated by an electrically driven actuator. Mathematically, the system will be modelled using partial delay differential equations (PDDEs). We believe that this is the first ever attempt to use PDDEs to represent a real-time dynamic substructuring experiment. It should be noted that the theory of PDDEs with applications to engineering systems is at its early stage in general, and neutral PDDEs in particular. The qualitative theory of partial functional differential equations with emphasis on reaction–diffusion equations with delay can be found in Wu (1996).

After reducing the system to the finite mode truncation of the beam, we analyse the dynamics of the model using the method of multiple scales, and derive the amplitude equation for the resonant case. The numerical simulations of the finite mode truncation of the delayed beam equation are performed and subsequently compared with the experimental results. We present the experimental response of the beam to the excitation with different time delays, which show periodic and quasi-periodic behaviour. Also, experimental and theoretical amplitude response diagrams are compared.

Section 2 introduces the equation of motion of the beam-MSD system. In §3 the multiple scales method is used to derive the amplitude response relation. Section 4 is devoted to the stability analysis of the neutral DDE, and stability regions in the parameter plane are identified. The numerical simulations of the delayed system are presented in §5. In §6 the experimental results are given and compared with the analytical and numerical findings. The paper concludes with the summary in §7.

2. Analytical formulation of the problem

The system under investigation is a cantilever steel beam clamped at one end and free at the other with a MSD attached to the free end of the beam. The equations of motion of the coupled system can be written as

$$\left(M\frac{\partial^2 u}{\partial t^2}(x,t)+C\frac{\partial u}{\partial t}(x,t)+Ku(x,t)\right)\delta(x-L)$$
$$+\,m\frac{\partial^2 u}{\partial t^2}(x,t)+EI\frac{\partial^4 u}{\partial x^4}(x,t)=A\sin(\omega t)\delta(x-L), \tag{2.1}$$

where x is the coordinate along the beam, t is the time, L denotes the undeformed length of the beam and m is the mass. Furthermore, δ is the Dirac delta function, EI is constant, M, C and K are the mass, damping and stiffness coefficients of the oscillator, respectively. A MSD is attached to the free end of the beam. An external force is acting on the MSD with amplitude A and frequency ω, which in turn excites the beam.

The emulated, or real, system is divided and the MSD is taken to be the numerical model while the beam is constructed in the laboratory. The two parts are connected via an electrical actuator. This means that there is a delay between the time a signal is sent and the moment the displacement of the beam is received back. The schematic description of the model is presented in figure 1, and the details of the corresponding experimental loop are shown in figure 2. Therefore, the modified equation of motion has the form

$$\left(M\frac{\partial^2 u}{\partial t^2}(x,t)+C\frac{\partial u}{\partial t}(x,t)+Ku(x,t)\right)\delta(x-L)$$
$$+\,m\frac{\partial^2 u}{\partial t^2}(x,t-\tau)+EI\frac{\partial^4 u}{\partial x^4}(x,t-\tau)=A\sin(\omega t)\delta(x-L), \tag{2.2}$$

where τ is the time delay (assumed to be constant).

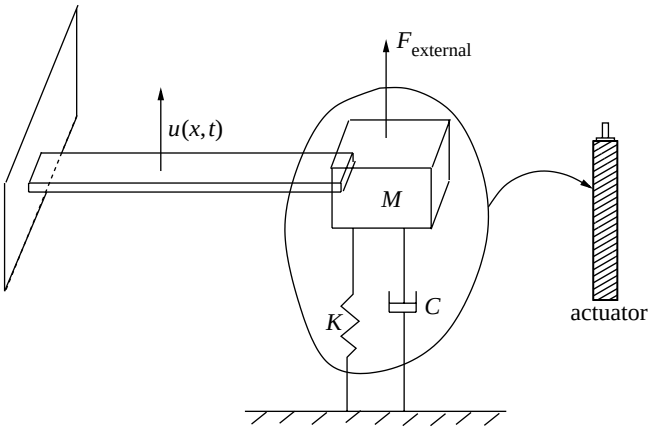

Figure 1. Schematic description of the coupled beam-MSD system.

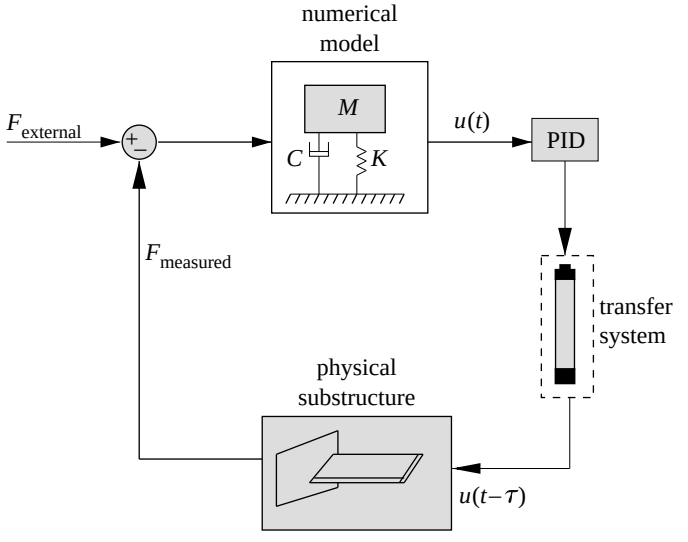

Figure 2. Schematic description of an experimental loop.

To simplify equation (2.2), one can introduce the following non-dimensional quantities:

$$\tilde{t} = \omega_0 t, \quad \tilde{x} = \frac{x}{L}, \quad \tilde{\tau} = \omega_0 \tau, \quad \omega_0^2 = \frac{EI}{mL^4}.$$

Under this rescaling and omitting tildes, equation (2.2) can be rewritten in the form

$$\left(\frac{\partial^2 u}{\partial t^2}(x,t) + 2\zeta \frac{\partial u}{\partial t}(x,t) + \kappa^2 u(x,t)\right)\delta(x-1)$$

$$+ \mu \frac{\partial^2 u}{\partial t^2}(x,t-\tau) + \mu \frac{\partial^4 u}{\partial x^4}(x,t-\tau) = \alpha \sin(\omega t)\delta(x-1), \tag{2.3}$$

where

$$\zeta = \frac{C}{2M\omega_0}, \quad \kappa = \sqrt{\frac{K}{M\omega_0^2}}, \quad \mu = \frac{m}{M} \quad \text{and} \quad \alpha = \frac{A}{M\omega_0^2}.$$

An approximate series solution of equation (2.3) can be taken to be in the form (Gürgöze 1998)

$$u(x,t) = \sum_{m=1}^{n} u_m(x) q_m(t),$$

where $u_m(x)$ are the orthogonal eigenfunctions of the clamped-free beam without an MSD, normalized with respect to the mass density. Functions $q_m(t)$ represent the unknown time-dependent generalized coordinates. Upon substituting the expansion of the solution $u(x, t)$ into equation (2.3), multiplying both sides by the kth eigenfunction $u_k(x)$ and integrating over the rescaled beam length, we obtain the set of DDEs

$$u_k(1)\sum_{m=1}^{n} u_m(1)\ddot{q}_m(t) + 2\zeta u_k(1)\sum_{m=1}^{n} u_m(1)\dot{q}_m(t) + \kappa^2 u_k(1)\sum_{m=1}^{n} u_m(1) q_m(t) + \mu\ddot{q}_k(t-\tau) + \mu\beta_k^4 q_k(t-\tau) = \alpha u_k(1)\sin\omega t, \quad k = 1, \ldots, n, \tag{2.4}$$

where the eigenvalues β_i are solutions of the transcendental equation

$$\cosh\beta_i \cos\beta_i + 1 = 0, \quad i = 1, 2, \ldots,$$

with $\beta_1 \approx 1.8751$.

Assuming that the dynamics of the beam is well represented by that of its first mode, we can reduce the system (2.4) to one second-order neutral DDE (as it involves time-delayed highest derivative)

$$u_1^2(1)\ddot{q}_1(t) + 2\zeta u_1^2(1)\dot{q}_1(t) + \kappa^2 u_1^2(1) q_1(t) + \mu\ddot{q}_1(t-\tau) + \mu\beta_1^4 q_1(t-\tau) = \alpha u_k(1)\sin\omega t, \tag{2.5}$$

where

$$u_1(x) = \cosh\beta_1 x - \cos\beta_1 x - \gamma_1(\sinh\beta_1 x - \sin\beta_1 x), \quad \gamma_1 = \frac{\cosh\beta_1 + \cos\beta_1}{\sinh\beta_1 + \sin\beta_1}.$$

We can further recast equation (2.5) as

$$\ddot{q}_1(t) + 2\zeta\dot{q}_1(t) + \kappa^2 q_1(t) + \mu^*\ddot{q}_1(t-\tau) + \upsilon q_1(t-\tau) = \alpha^*\sin\omega t, \tag{2.6}$$

where

$$\mu^* = \frac{\mu}{u_1^2(1)}, \ \upsilon = \mu^*\beta_1^4, \text{ and } \alpha^* = \frac{\alpha}{u_1(1)}.$$

Equation (2.6) is the equation whose properties will be investigated in this paper.

3. Perturbation analysis

In order to analyse the primary resonance of the neutral delay equation (2.6) using the method of multiple scales (Nayfeh & Pai 2004), we confine the study to the case of small damping, weak feedback and soft excitation. This means that

we assume the following:

$$\zeta = \mathcal{O}(\varepsilon), \quad \mu^* = \mathcal{O}(\varepsilon), \quad \alpha^* = \mathcal{O}(\varepsilon), \quad \upsilon = \mathcal{O}(\varepsilon), \quad \omega - \kappa = \varepsilon\sigma \quad \text{and} \quad \sigma = \mathcal{O}(1),$$

where ε is small and σ is a detuning parameter. We look for the solution as a two-scale expansion

$$q(t) = \nu_0(T_0, T_1) + \varepsilon\nu_1(T_0, T_1) + \mathcal{O}(\varepsilon^2), \tag{3.1}$$

where $T_0 = t$ and $T_1 = \varepsilon t$. We use the following differential operators:

$$\frac{\mathrm{d}}{\mathrm{d}t} = \frac{\partial}{\partial T_0} + \varepsilon\frac{\partial}{\partial T_1} \equiv D_0 + \varepsilon D_1 + \mathcal{O}(\varepsilon^2), \qquad \frac{\mathrm{d}^2}{\mathrm{d}t^2} = D_0^2 + 2\varepsilon D_0 D_1 + \mathcal{O}(\varepsilon^2). \tag{3.2}$$

Substituting expansion (3.1) into (2.6) and using the differential operators (3.2) gives (by equating powers of ε) a set of linear partial DDEs. The zeroth and first-order approximations are

$$D_0^2\nu_0(T_0, T_1) + \kappa^2\nu_0(T_0, T_1) = 0, \tag{3.3}$$

and

$$\begin{aligned} D_0^2\nu_1(T_0, T_1) + \kappa^2\nu_1(T_0, T_1) = &-2D_0D_1\nu_0(T_0, T_1) - 2\zeta D_0\nu_0(T_0, T_1) \\ &-\mu^* D_0^2\nu_0(T_0 - \tau, T_1) - \upsilon\nu_0(T_0 - \tau, T_1) \\ &+ \alpha^*\sin(\kappa T_0 + \sigma T_1). \end{aligned} \tag{3.4}$$

Solving equation (3.3), we have

$$\nu_0(T_0, T_1) = A(T_1)\mathrm{e}^{\mathrm{i}\kappa T_0} + \text{c.c.}, \tag{3.5}$$

where c.c. stands for complex conjugate, and

$$A(T_1) = \frac{1}{2}\alpha(T_1)\mathrm{e}^{\mathrm{i}\kappa\beta(T_1)}. \tag{3.6}$$

Using ν_0 from equation (3.5) in (3.4) gives

$$\begin{aligned} D_0^2\nu_1(T_0, T_1) + \kappa^2\nu_1(T_0, T_1) = &-2\mathrm{i}\kappa D_1 A\mathrm{e}^{\mathrm{i}\kappa T_0} - 2\zeta\kappa\mathrm{i}A\mathrm{e}^{\mathrm{i}\kappa T_0} - \upsilon A\mathrm{e}^{\mathrm{i}\kappa T_0}\mathrm{e}^{-\mathrm{i}\tau\kappa} \\ &+ \kappa^2\mu^* A\mathrm{e}^{-\mathrm{i}\tau\kappa}\mathrm{e}^{\mathrm{i}\kappa T_0} + \frac{\alpha^*}{2}\mathrm{e}^{\mathrm{i}\sigma T_1}\mathrm{e}^{\mathrm{i}\kappa T_0} + \text{c.c.} \end{aligned} \tag{3.7}$$

To eliminate the secular terms in equation (3.7), we set

$$-2\mathrm{i}\kappa(D_1 + \zeta)A + \kappa^2\mu^* A(T_1)\mathrm{e}^{-\mathrm{i}\tau\kappa} - \upsilon A\mathrm{e}^{-\mathrm{i}\tau\kappa} + \frac{\alpha^*}{2}\mathrm{e}^{\mathrm{i}\sigma T_1} = 0.$$

Substituting equation (3.6) into the last expression and separating into the real and imaginary parts gives

$$D_1\alpha = -\frac{1}{2\kappa}\left[\mu^*\kappa^2\alpha\sin\kappa\tau - \alpha^*\sin(\sigma T_1 - \beta\kappa) - \upsilon\alpha\sin\kappa\tau + 2\zeta\kappa\alpha\right],$$

$$\alpha D_1\beta = -\frac{1}{2\kappa^2}\left[\mu^*\alpha\kappa^2\cos\kappa\tau - \upsilon\alpha\cos\kappa\tau + \alpha^*\cos(\sigma T_1 - \beta\kappa)\right].$$

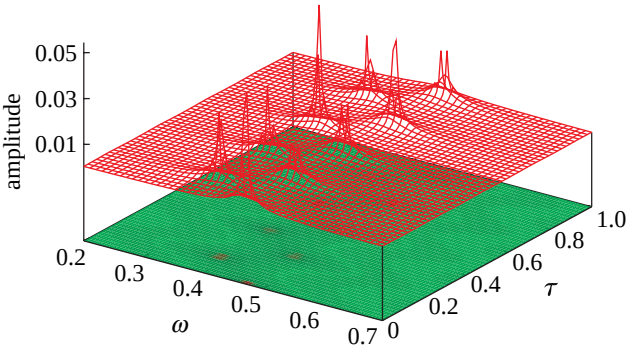

Figure 3. Amplitude response as a function of time delay and frequency of the perturbation.

Moreover, if we introduce a phase φ such that $\varphi=\sigma T_1-\beta(T_1)\kappa$, then the equations governing the amplitude $\alpha(T_1)$ and the phase $\varphi(T_1)$ take the form

$$D_1\alpha = \frac{1}{2\kappa}(\upsilon \sin \kappa\tau - \mu^*\kappa^2 \sin \kappa\tau - 2\zeta\kappa)\alpha + \frac{\alpha^*}{2\kappa}\sin\varphi,$$
$$\alpha D_1\varphi = \frac{1}{2\kappa^2}(\sigma\kappa^2 + \upsilon\cos\kappa\tau - \mu^*\kappa^2\cos\kappa\tau)\alpha - \frac{\alpha^*}{2\kappa^2}\cos\varphi. \tag{3.8}$$

Obviously, the presence of time delay τ in the original equation modifies the averaged equations by adding additional terms.

Steady-state solutions of equation (2.6) for the primary resonance correspond to the fixed points of equations (3.8) and these can be obtained by setting $D_1\alpha=0$ and $D_1\varphi=0$. This leads to a set of algebraic equations (assuming $\alpha\neq0$)

$$(\upsilon \sin \kappa\tau - \mu^*\kappa^2 \sin \kappa\tau - 2\zeta\kappa)\alpha + \alpha^*\sin\varphi = 0,$$
$$(\sigma\kappa^2 + \upsilon\cos\kappa\tau - \mu^*\kappa^2\cos\kappa\tau)\alpha - \alpha^*\cos\varphi = 0.$$

From the last system of equations, we can derive the frequency response relations between the amplitude α and σ and the phase φ and σ,

$$\alpha = \frac{\alpha^*}{[(\upsilon \sin \kappa\tau - \mu^*\kappa^2 \sin \kappa\tau - 2\zeta\kappa)^2 + (\sigma\kappa^2 + \upsilon\cos\kappa\tau - \mu^*\kappa^2\cos\kappa\tau)^2]^{1/2}}$$
$$\tan\varphi = -\frac{(\upsilon \sin \kappa\tau - \mu^*\kappa^2 \sin \kappa\tau - 2\zeta\kappa)}{(\sigma\kappa^2 + \upsilon\cos\kappa\tau - \mu^*\kappa^2\cos\kappa\tau)}. \tag{3.9}$$

These expressions will be used later when comparing analytical and experimental amplitude responses.

The extreme values of the amplitude are

$$\alpha_{\text{extr}} = \frac{\alpha^*}{\upsilon - \mu^*\kappa^2 \pm \kappa\sqrt{\sigma^2\kappa^2 + 4\zeta^2}}, \tag{3.10}$$

and they are attained at

$$\tau_m^{\text{extr}} = \arctan\left(-\frac{2\zeta}{\sigma\kappa}\right) + m\pi, \quad m = 1, 2, \ldots.$$

Figure 3 illustrates the amplitude response as given by the expression (3.9) for different delay times. One can observe that there are two nearby perturbation frequencies that exert the largest response of the system. In the vicinity of those two frequencies, which correspond to the absolute maxima of the response, the system also has peaks in the amplitude response whose position depends on the perturbation frequency and time delay as given by expression (3.10).

4. Stability analysis

Returning to equation (2.6), the characteristic equation for the trivial solution has the form

$$\lambda^2 + 2\zeta\lambda + \kappa^2 + \mu^*\lambda^2 \mathrm{e}^{-\lambda\tau} + \upsilon \mathrm{e}^{-\lambda\tau} = 0.$$

Purely imaginary eigenvalues occur when $\lambda = \pm \mathrm{i}\psi$, $\psi \neq 0$ with

$$-\psi^2 + 2\mathrm{i}\zeta\psi + \kappa^2 - \mu^*\psi^2 \mathrm{e}^{-\mathrm{i}\psi\tau} + \upsilon \mathrm{e}^{-\mathrm{i}\psi\tau} = 0.$$

Separating the last equation into the real and imaginary parts gives

$$\psi_\pm = \frac{1}{1-\mu^{*2}}\left[(2\zeta^2 - \kappa + \mu^*\upsilon) \pm \sqrt{(2\zeta^2 - \kappa + \mu^*\upsilon)^2 - (\kappa^4 - \upsilon^2)(1-\mu^{*2})}\right], \quad (4.1)$$

and

$$\tau = \frac{1}{\psi_\pm}\left[\arccos\frac{\psi_\pm^2 - \kappa^2}{\upsilon - \mu^*\psi_\pm^2} \pm 2\pi n\right], \quad n = 1, 2, \ldots.$$

Figure 4 shows the stability boundary in the parameter plane of the time delay τ and the mass ratio μ^* for different values of κ and ζ. The values of μ^* (i.e. the mass ratio of mass of the beam to the mass of the MSD) do not exceed 1 as for $|\mu^*| > 1$ the trivial steady state is unstable for any delay time (Kyrychko *et al.* 2006). One can note that the increase of the spring stiffness leads to the shift of the stability boundary to the left, and also to a slight decrease in the critical value of μ^*. The stable region becomes smaller and narrower. On the other hand, when the damping coefficient increases, the horizontal position of the stability boundary remains unchanged, while both the peaks and the bottoms on the curve grow. These changes in the stability boundary provide important information needed for the design of a stable experiment. Moreover, they indicate how varying the values of parameters of the numerical model can stabilize the system.

For a detailed description of the stability switches and an extensive stability study of neutral DDEs, the reader is referred to Kyrychko *et al.* (2006).

5. Numerical simulations

This section is devoted to the numerical simulations of the neutral delay equation (2.6) and then the system (2.4). Equation (2.6) was discretized with an explicit finite difference scheme; to improve numerical stability of the scheme, the damping term was approximated by central differences. In all simulations, the values of the damping coefficient ζ, rescaled stiffness of the oscillator κ and

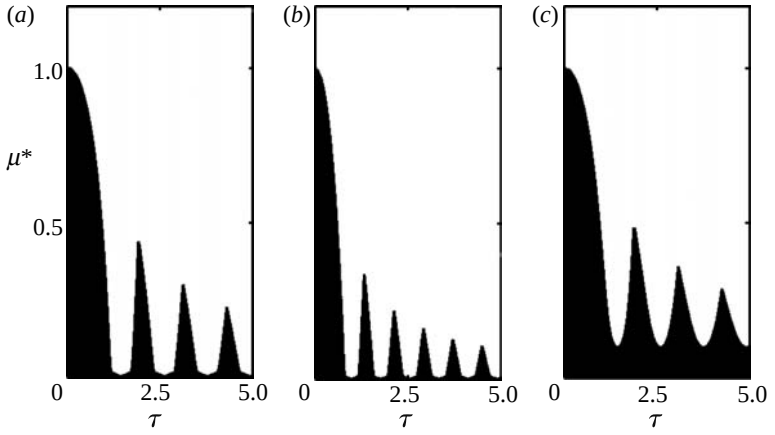

Figure 4. Stability boundary: (*a*) $\kappa=5.4$, $\zeta=0.003$; (*b*) $\kappa=8$, $\zeta=0.003$; (*c*) $\kappa=5.4$, $\zeta=0.153$. Black region is a stable region and area above it is an unstable region.

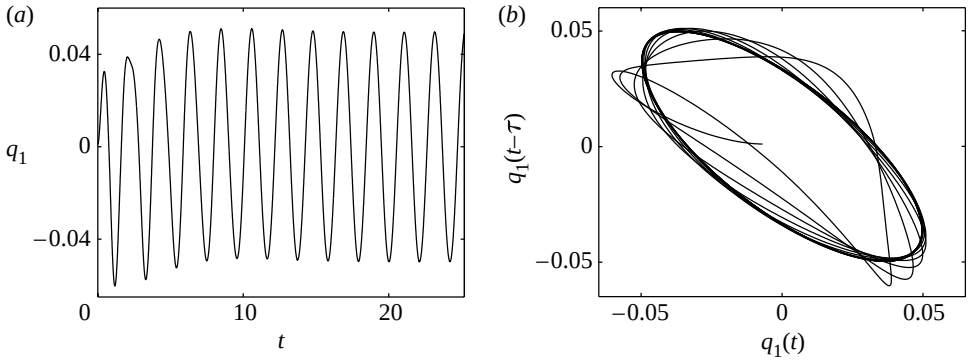

Figure 5. Solution $q_1(t)$ of equation (2.6) with delay time $\tau=0.8$. (*a*) Temporal dynamics. (*b*) Phase portrait in the plane $(q_1(t),\ q_1(t-\tau))$.

the rescaled ratio of mass of the beam to the mass of the MSD μ^* were taken to be constant. The values used in figures 5–7 are $\zeta=0.003$, $\kappa=5.4$ and $\mu^*=0.6$. In principle, these values can vary, since the parameters of the MSD can easily be changed as they are represented by a numerical model in the experiment. We have tried different combinations of parameters in our numerical simulations and the results are robust and qualitatively similar to those presented in this paper. The equation was forced with an amplitude $\alpha^*=1$ and frequency $\omega=5$. The time delay was varied, starting with a value of $\tau=0.8$. As the trivial steady state of the unforced equation (2.6) is linearly asymptotically stable, external forcing transforms it into a stable periodic orbit. The result of this simulation is shown in figure 5 together with a corresponding phase plane.

For a larger value of the time delay $\tau=0.9$, the stability of the steady state is lost and the solution develops into a quasi-periodic orbit shown in figure 6. Figure 7 illustrates the solution of equation (2.6) when the time delay is increased further. The solution is unstable and is characterized by a fast growth of the amplitude of oscillations.

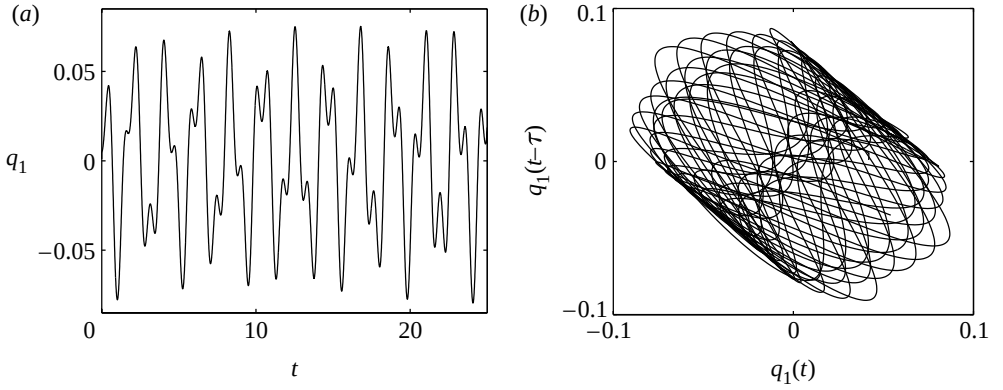

Figure 6. Solution $q_1(t)$ of equation (2.6) with delay time $\tau=0.9$. (*a*) Temporal dynamics. (*b*) Phase portrait in the plane $(q_1(t),\ q_1(t-\tau))$.

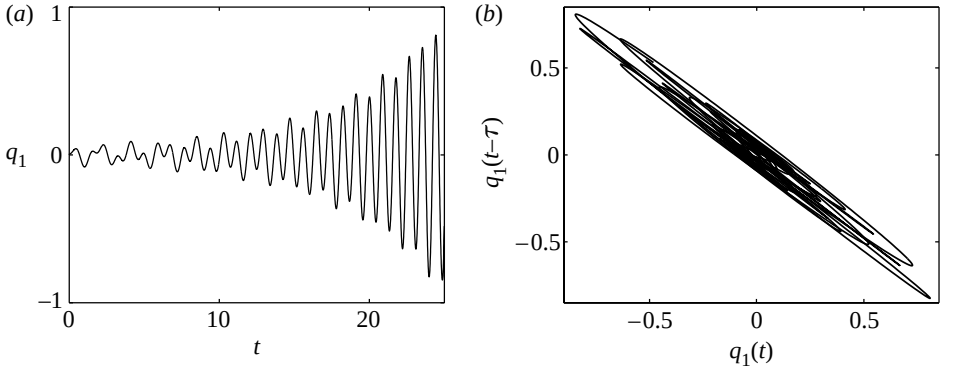

Figure 7. Solution $q_1(t)$ of equation (2.6) with delay time $\tau=1.2$. (*a*) Temporal dynamics. (*b*) Phase portrait in the plane $(q_1(t),\ q_1(t-\tau))$.

To demonstrate the full spatio-temporal dynamics of the beam-MSD system under external excitation, we solve the system (2.4) numerically. For illustration purposes, the number of modes in the expansion is taken to be three. One end of the beam is fixed, while the MSD is attached to the other one. The applied external forcing makes the free end of the beam vibrate. In figure 8*a*, the value of the delay time is $\tau=0.8$. One can observe the influence of the higher beam modes which lead to a non-monotonicity of the profile. For $\tau=0.9$, the beam profile remains qualitatively similar but the quasi-periodic nature of the temporal component induces a complex dynamics as shown in figure 8*b*.

6. Experimental set-up

In order to confirm our analytical investigations, real-time dynamic substructuring tests are carried out. As discussed earlier, the steel beam is taken to be the physical substructure part, and the MSD is modelled numerically. The numerical model will be used to calculate the displacement at the interface due to external forcing. This displacement is then applied to the beam in real time using an electro-mechanical

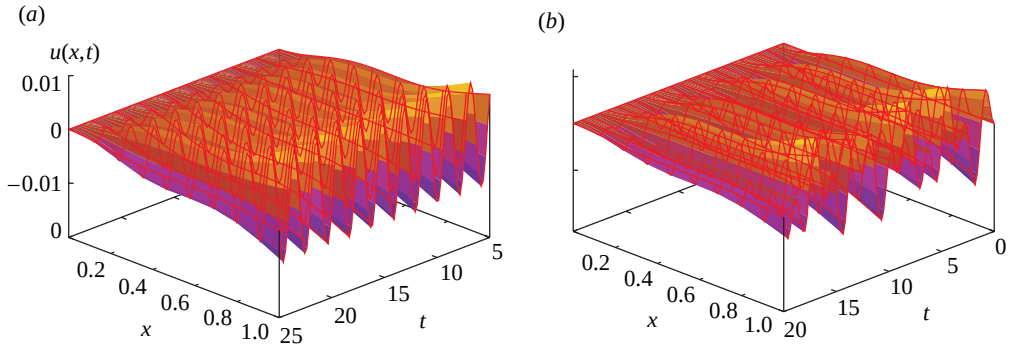

Figure 8. Spatio-temporal dynamics of a three-mode truncation of the beam equation with (*a*) $\tau=0.8$ and (*b*) $\tau=0.9$.

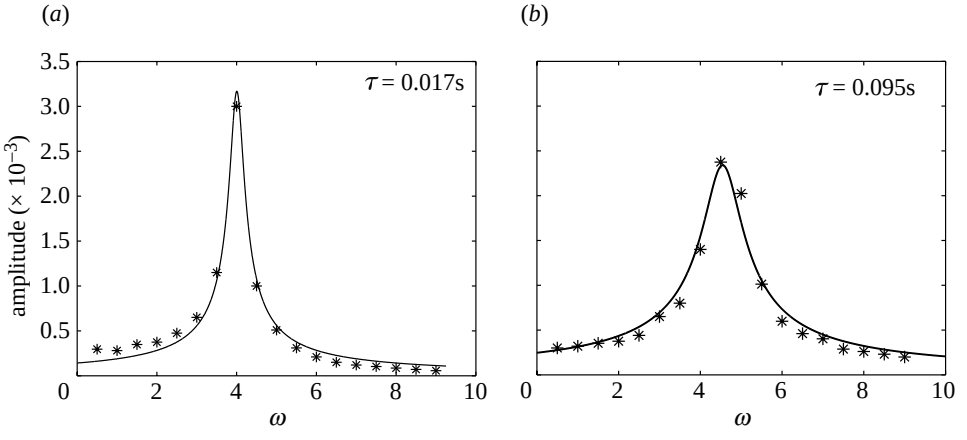

Figure 9. Amplitude response plot. Solid line is the theoretical prediction from equation (3.9); stars show experimental points.

actuator. The beam is mounted on the heavy frame to reduce noise and other unwanted effects. One end of the beam is screwed to the frame and an actuator is mounted on the free end of the beam. The force acting on the beam is measured using a load cell, a linear variable differential transformer (LVDT) displacement transducer is used to track and control the movements of the actuator and a digital incremental encoder records the vertical displacement of the beam. In order to implement a real-time testing, we use a dSpace DS1104 RD Controller board and MATLAB/Simulink are used to program a numerical model.

The beam has a fixed length of 1 m with width 5 cm and thickness 5 mm. The mass, stiffness and damping of the numerical model will be varied during the experiment. First, we take $M=5$ kg, $C=1$ kg s^{-1} and $K=3500$ N m^{-1}. The amplitude of the external excitation is $A=6$ N and frequency is set to be 2 Hz. In figure 9, the amplitude response of the system is shown. The solid line represents an analytical amplitude and the stars are experimental points. Figure 9*a*,*b* is plotted for two different time delays, namely, $\tau=0.017$ and 0.095 s. The original time delay in the system is 0.017 s. We can see from figure 9*b* that increasing the

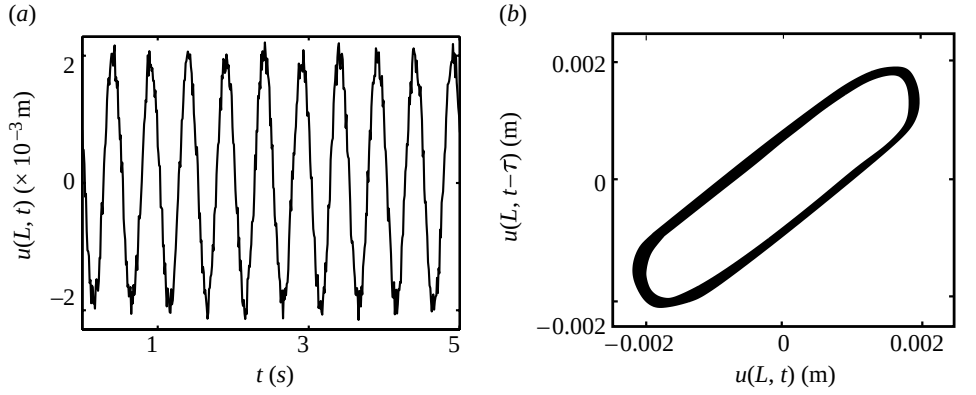

Figure 10. Experimental displacement of the free end of the beam for $\tau = 0.067$ s. (*a*) Temporal dynamics. (*b*) Phase portrait in the plane $(u(L, t), u(L, t-\tau))$.

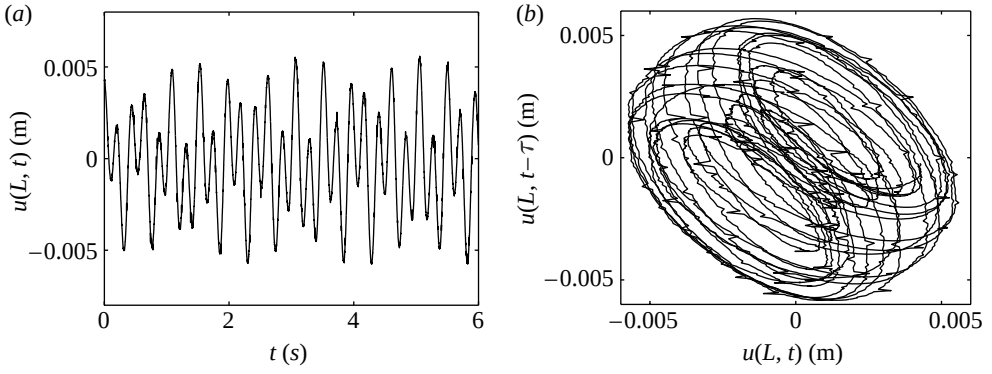

Figure 11. Experimental displacement of the free end of the beam for $\tau = 0.072$ s. (*a*) Temporal dynamics. (*b*) Phase portrait in the plane $(u(L, t), u(L, t-\tau))$.

time delay decreases the peak amplitude by approximately 30%. The experimental points closely follow the theoretical curve which shows a very good accuracy of the analytical predictions.

For the experimental results shown in figures 10–12, we fix all parameters of the system and increase the time delay. The external force is applied to the numerical model and then the excitation is sent to the free end of the beam. Figure 10 shows periodic oscillations of the beam displacement at the free end for a small time delay. As the time delay is increased, the system undergoes a transition into quasi-periodic motion due to the loss of stability of the trivial steady state as shown in figure 11*a*. These oscillations are robust against external perturbation, i.e. they do not change to periodic motion if an additional disturbance is applied at the free end of the beam. In this case, the dynamics is characterized by large excursions in the phase space (figure 11*b*). As the time delay is increased further, the quasi-periodic oscillations persist but their amplitude grows. This results in very large transversal displacements of the beam and eventually the system becomes unstable. This regime is illustrated in figure 12. Comparing the numerical simulations presented in figures 5–7 with the experimental results of this section, it

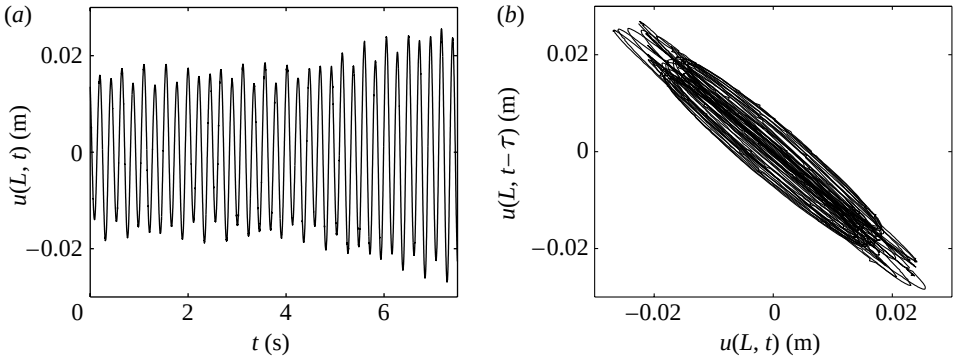

Figure 12. Experimental displacement of the free end of the beam for $\tau = 0.112$ s. (*a*) Temporal dynamics. (*b*) Phase portrait in the plane $(u(L,\ t),\ u(L,\ t-\tau))$.

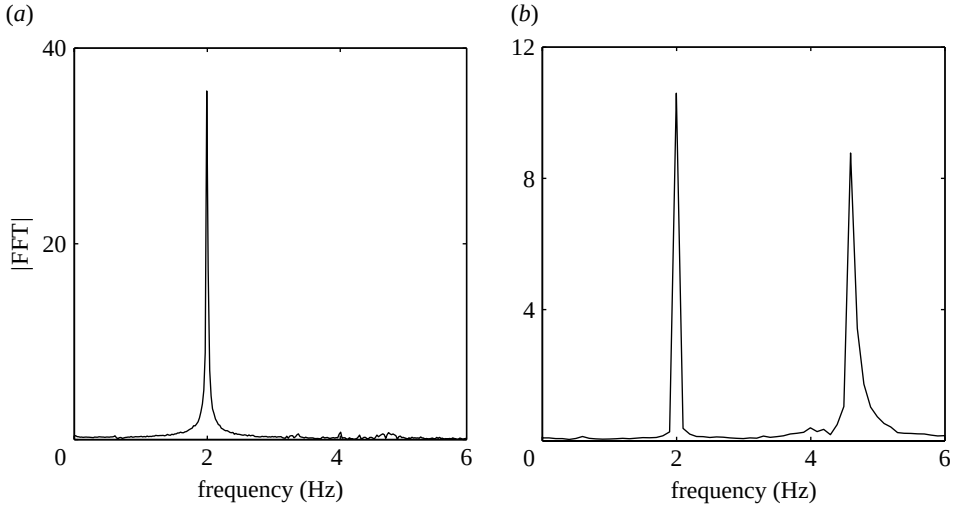

Figure 13. Snapshots of the Fourier spectrum of the experimental displacement of the free end of the beam for different delays. (*a*) $\tau = 0.067$ s and (*b*) $\tau = 0.072$ s.

is worth noting that even the first-mode approximation of the full model captures the essential dynamics of the system. Periodic, quasi-periodic and unstable regimes occur in numerical simulations at the values of time delay (in original non-rescaled time units) $\tau \approx 0.07$, 0.0787 and 0.105 s when compared with experimental values of $\tau \approx 0.067$, 0.072 and 0.112 s, respectively.

In figure 13, we have plotted the Fourier transform of the experimental signals given in figures 10 and 11. In figure 13*a*, when $\tau \approx 0.067$ s, we observe one main frequency in the Fourier spectrum that corresponds to the frequency of external excitation of 2 Hz. For a larger time delay $\tau \approx 0.072$ s, there are two frequencies present in the spectrum as shown in figure 13*b*. One of them at 2 Hz is a forcing frequency, and the other at $\omega \approx 4.59$ Hz (analytical value $\omega \approx 4.65$ Hz) is the Hopf frequency that appears when a trivial steady state loses its stability for larger time delay. The Fourier transform of the signal presented in figure 12 is qualitatively similar to the one plotted in figure 13*b*.

7. Conclusions

This paper deals with modelling of the real-time dynamic experiment of a spatially extended system. The system consists of a steel beam clamped at one end and a MSD attached to the free end. This system has been substructured by taking the beam to be the physical structure and a MSD replaced by its numerical counterpart. The transfer system used to connect real and 'virtual' parts is an actuator which introduces delays into the experiment. The model equations of motion are given by a partial differential equation with time delay. It is well known that time delays induce instability, and analytical treatment of the system allows one to find the regions of system stability and their variation depending on the parameters of the MSD. The significant advantage of this experimental technique is that these parameters can easily be varied as they are defined in the numerical part of the experiment. Time delay is an unwanted effect in hybrid testing experiments. However, the fact that it can be varied during the experiment allows one to switch between different stability regions. The stability areas can be very small and narrow making them harder to find when running an experiment, but the use of the theoretical stability predictions gives insights into their location.

Using the method of multiple scales, we find an amplitude response relation of the system depending on the time delay. This is then verified experimentally giving excellent agreement. We observe that changing the time delay helps to reduce the amplitude response peaks. Numerical simulations of an externally forced system demonstrate periodic and quasi-periodic behaviour in different parameter regions. This again gives good correspondence to the experimental observations.

The analytical, numerical and experimental results for the beam-MSD system considered in this paper provide important information on the behavioural changes in system dynamics with respect to time delays that are always present in the real-time dynamic experiments. These findings provide much needed insights into the problems and their solutions in the case of large-scale experiments.

The authors would like to acknowledge the support of the EPSRC: Y.K. is supported by EPSRC grant (GR/72020/01), A.G.B. is supported by EPSRC grant (GR/S49780) and D.J.W. via an Advanced Research Fellowship.

References

Adimy, M., Ezzinbi, K. & Ouhinou, A. 2006 Variation of constants formula and almost periodic solutions for some partial functional differential equations with infinite delay. *J. Math. Anal. Appl.* **317**, 668–689. (doi:10.1016/j.jmaa.2005.07.002)

Blakeborough, A., Williams, M. S., Darby, A. P. & Williams, D. M. 2001 The development of real-time substructure testing. *Phil. Trans. R. Soc. A* **359**, 1869–1891. (doi:10.1098/rsta.2001.0877)

Ercoli, L. & Laura, P. A. A. 1987 Analytical and experimental investigation of continuous beams carrying elastically mounted masses. *J. Sound Vib.* **114**, 519–533. (doi:10.1016/S0022-460X(87)80021-4)

Gürgöze, M. 1996 On the eigenfrequencies of a cantilever beam with attached tip mass and a spring-mass system. *J. Sound Vib.* **190**, 149–162. (doi:10.1006/jsvi.1996.0053)

Gürgöze, M. 1998 On the sensitivities of the eigenvalues of a viscously damped cantilever carrying a tip mass. *J. Sound Vib.* **216**, 215–225. (doi:10.1006/jsvi.1998.1586)

Hu, H. Y. & Wang, Z. H. 2002 *Dynamics of controlled mechanical systems with delayed feedback*. Berlin, Germany: Springer.

Kyrychko, Y. N., Blyuss, K. B., Gonzalez-Buelga, A., Hogan, S. J. & Wagg, D. J. 2006 Real-time dynamic substructuring in a coupled oscillator-pendulum system. *Proc. R. Soc. A* **462**, 1271–1294. (doi:10.1098/rspa.2005.1624)

Laurent, T., Rider, B. & Reed, M. 2006 Parabolic behavior of a hyperbolic delay equation. *SIAM J. Math. Anal.* **38**, 1–15. (doi:10.1137/040611422)

Nayfeh, A. H. & Pai, P. F. 2004 *Linear and nonlinear structural mechanics*. New York, NY: Wiley-Interscience.

Rossi, R. E., Laura, P. A. A., Avalos, D. R. & Larrondo, H. 1993 Free vibration of Timoshenko beams carrying elastically mounted concentrated masses. *J. Sound Vib.* **165**, 209–223. (doi:10.1006/jsvi.1993.1254)

Sieber, J. & Krauskopf, B. In press. Control-based continuation of periodic orbits with a time-delayed difference scheme. *Int. J. Bifurcation and Chaos*.

Wallace, M. I., Sieber, J., Neild, S. A., Wagg, D. J. & Krauskopf, B. 2005 Delay differential equation models for real-time dynamic substructuring. *Earthq. Eng. Struct. Dyn.* **34**, 1817–1832. (doi:10.1002/eqe.513)

Williams, M. S. & Blakeborough, A. 2001 Laboratory testing of structures under dynamic loads: an introductory review. *Phil. Trans. R. Soc. A* **359**, 1651–1669. (doi:10.1098/rsta.2001.0880)

Wu, J. 1996 *Theory and applications of partial functional differential equations*. New York, NY: Springer.